

Using the forward movement of a container ship navigating in the Arctic to air-cool a marine organic Rankine cycle unit

Santiago Suárez de la Fuente^{a,1}, Ulrik Larsen^b, Rachel Pawling^a, Iván García Kerdan^c, Alistair Greig^a and Richard Bucknall^a

^aUniversity College London, Department of Mechanical Engineering, Roberts Building, Torrington Place, London, WC1E 7JE, United Kingdom

^bChalmers University of Technology, Maritime Operations, 412 96 Gothenburg, Sweden

^cCentre for Process Systems Engineering, Imperial College London, Roderic Hill Building South Kensington Campus, London, SW7 2AZ, UK

Abstract

Ice coverage in the Arctic is declining, opening up new shipping routes which can drastically reduce voyage lengths between Asia and Europe. There is also a drive to improve the ships' energy efficiency to meet international emissions design regulations such as the mandated Energy Efficiency Design Index. The organic Rankine cycle (ORC) is one thermodynamic cycle that is being actively examined to improve ships' design and operational efficiency.

Low heat sink temperatures can significantly increase waste heat recovery systems thermal efficiency. In Arctic regions, the ambient air temperature can be much lower than the sea temperature, presenting interesting opportunities. However, using air as cooling medium requires larger condensers and power compared to a water-cooled system.

This paper investigates the exploitation of the forward movement of a container ship navigating in the Arctic Circle and density-change induced flows as means of moving air through the condenser to reduce the fan power required. The ORC unit uses the scavenge air available waste heat to produce electric power. A two-step optimisation method is used with the objective of minimising the ship annual CO₂ emissions. The results suggest that the supportive cooling could reduce the fan power by up to 60%, depending on ambient air temperature.

Keywords: Shipping; Arctic; Efficiency; CO₂ emission reductions; Air-cooling; Waste heat recovery systems;

¹ Corresponding author. Tel.: +44-20-7679-7063.
E-mail address: santiago.fuente.11@ucl.ac.uk

Nomenclature

Symbol	Name	Units	Symbol	Name	Units
A	Area	m^2	H_{NPL}	Height from midpoint of lower opening to neutral pressure level	m
a	Pump tuning coefficient	-	\dot{m}	Mass flow rate	kg/s
b	Pump tuning coefficient	-	MT	Monthly trips	-
C	Opening effectiveness	-	N	Rotational speed	RPM
c	Pump tuning coefficient	-	OM	Number of months	-
C_D	Discharge coefficient	-	OS	Number of operating speeds	-
C_F	Carbon factor	t CO ₂ /t fuel	OW	Number of wind conditions	-
c_p	Specific heat at constant pressure	kJ/kg·K	P	Pressure	kPa
C_P	Pressure coefficient	-	\dot{Q}	Heat transfer rate	kW
CS	Carbon savings	t/h	$SFOC$	Specific fuel oil consumption	g/kWh
C_T	Expander constant	kg·K ^{0.5} /kPa·s	t	Time	h
d	Diameter	m	T	Temperature	K
d	Pump tuning coefficient	-	v	Speed	m/s
E	Electrical Energy	kWh _e	\dot{V}	Volumetric flow rate	m ³ /s
g	Gravitational acceleration	m/s ²	\dot{W}	Power	kW
h	Specific enthalpy	kJ/kg			
Greek Symbol	Name	Units	Greek Symbol	Name	Units
θ	Apparent wind Angle	Degrees	η	Efficiency	%
ρ	Density	kg/m ³	Φ	True wind angle	°
Δ	Difference	-	Γ	True wind direction	°N

Subscripts and superscripts	Name	Subscripts and superscripts	Name
<i>a</i>	Apparent	<i>o</i>	Outlet/Outside
<i>amb</i>	Ambient	<i>off</i>	Off-design
<i>aux</i>	Auxiliary engine	<i>p</i>	Pump
<i>b</i>	Bottom	<i>s</i>	Ship
<i>ch</i>	Chimney	<i>S</i>	Stack
<i>co</i>	Condenser	<i>t</i>	True Wind Speed
<i>d</i>	Design	<i>T</i>	Total/Net
<i>e</i>	Electric/Electrical	<i>vr</i>	Venturi-shaped roof
<i>ex</i>	Expander	<i>wf</i>	Working fluid
<i>f</i>	Fan	<i>WH</i>	Waste heat
<i>g</i>	Generator	<i>WHRS</i>	Waste heat recovery system
<i>i</i>	Inlet	<i>ws</i>	Windscoop
<i>l</i>	Length		

Acronyms

Acronym	Definition	Acronym	Definition
AIS	Automatic Identification System	ORC	Organic Rankine Cycle
AWA	Apparent Wind Angle	SFC	Specific Fuel Consumption
AWS	Apparent Wind Speed	TEU	Twenty-foot Equivalent Unit
EEDI	Energy Efficiency Design Index	TWA	True Wind Angle
HFO	Heavy Fuel Oil	TWA	True Wind Direction
IMO	International Maritime Organization	TWS	True Wind Speed
LNG	Liquefied Natural Gas	WHB	Waste Heat Boiler
MCR	Maximum Continuous Rating	WHRS	Waste Heat Recovery System

1. Introduction

Recent studies show that ice coverage in the Arctic has been constantly declining [1,2] and suggest that it will continue to do so [3,4]. For shipping this opens up new routes which can drastically reduce voyage lengths between Asia and Europe. Schøyen and Bråthen [5] indicated a distance reduction of 37% when switching the Yokohama-London route from via the Suez canal to via the Arctic. Melia et al. [6] have used a selection of global climate models to predict Arctic sea ice reduction and anticipate the resulting increased opportunities for shipping in the region. In August 2017, the ice class Liquefied Natural Gas (LNG) carrier "*Christophe de Margerie*", completed her first voyage from Siberia to South Korea without the aid of an ice breaker [7]. She is the first of a fleet of 15 ships.

There is also a drive to improve the energy efficiency of ships to meet international emissions design regulations such as the International Maritime Organization (IMO) Energy Efficiency Design Index (EEDI). The EEDI entered into force on the first day of 2013 and is the only energy-efficiency measure that is legally binding across an entire global industry, applying to all countries [8]. Waste heat recovery systems (WHRS) is one efficiency measure that is actively being examined to improve ship propulsion efficiency and hence help ships satisfy their EEDI requirement [9].

Waste heat recovery systems have been identified as one of the most important technologies for reducing ships' fuel consumption and CO₂ emission [10]. Heat from the main engine exhaust gas is normally used to cover the steam demand and, when possible, produce mechanical or electrical power [11]. However, in Arctic operations, the increased on board heating demand precludes the use of an exhaust gas WHRS [12], leaving as an alternative waste heat candidate the engine charge air heat. From Figure 1, a waste heat boiler (WHB) extracts the available exhaust gas waste heat to produce steam which maintains operational temperatures for the ship's equipment when navigating in cold climates [13]. Looking at the turbocharger compressor, ambient air is compressed – using the wasted energy available in the exhaust gas flow via the turbocharger turbine – in order to increase the amount of air available for combustion inside the cylinder and increase its specific power output [14]. Due to the compression work, the incoming air increases its temperature and volume which reduces the mass of air entering the engine cylinder. To increase the amount of air mass, the charge air temperature is reduced via an air cooler before the engine intake manifold. The charge air waste heat represents about 17% of the fuel energy [14], and by substituting the air cooler for a WHRS boiler the wasted heat could be reutilised to produce power on board.

Mito et al. [15] calculated that by using the waste heat from the scavenge air in conjunction with the exhaust waste heat in a steam Rankine cycle, it is possible to save up to 1563 t of heavy fuel oil (HFO) per year if the main engine is constantly operated at its maximum continuous rating. These fuel savings represent an improvement in fuel consumption of 9.9% from the same ship without any WHRS installed. Charge air temperatures at design conditions are generally between 130°C and 150°C [16], but when considering the whole range of engine loading and ambient air temperatures, the range can be between

60°C up to 200°C as seen in MAN Diesel and Turbo [17]. This range of waste heat operating temperatures is suitable for Organic Rankine Cycle (ORC) units [18–20]. The use of the scavenge air waste heat has been explored by Suárez de la Fuente et al. [21] where the waste heat usage allowed a container ship to be in compliance with the EEDI regulation. Kalikatzarakis & Frangopoulos [22] used an ORC unit to take advantage of a ship main engine scavenge air waste heat in conjunction with other waste heat sources, with the WHRS manage to saving 1,050 t of CO₂. Shu et al. [23] performed a thermo-economic study of a marine ORC unit using the available waste heat for the main engine exhaust gas and also they considered the condenser’s design and performance impact. Integrating the operational profile to the design process, they calculated that an ORC unit using R123 as the working fluid would bring the largest cost-benefit for a containership, since it can operate at the fastest speed and with a waste heat temperature of 315°C, while R365mfc is more suitable to tankers and bulk carriers. An important point to highlight is that R123 and R365mfc are hydrochlorofluorocarbons and hydrofluorocarbons respectively. These refrigerants are soon to be phased out by the Montreal Protocol due to their high Global Warming Potential [24,25] and are not suitable for Arctic operations.

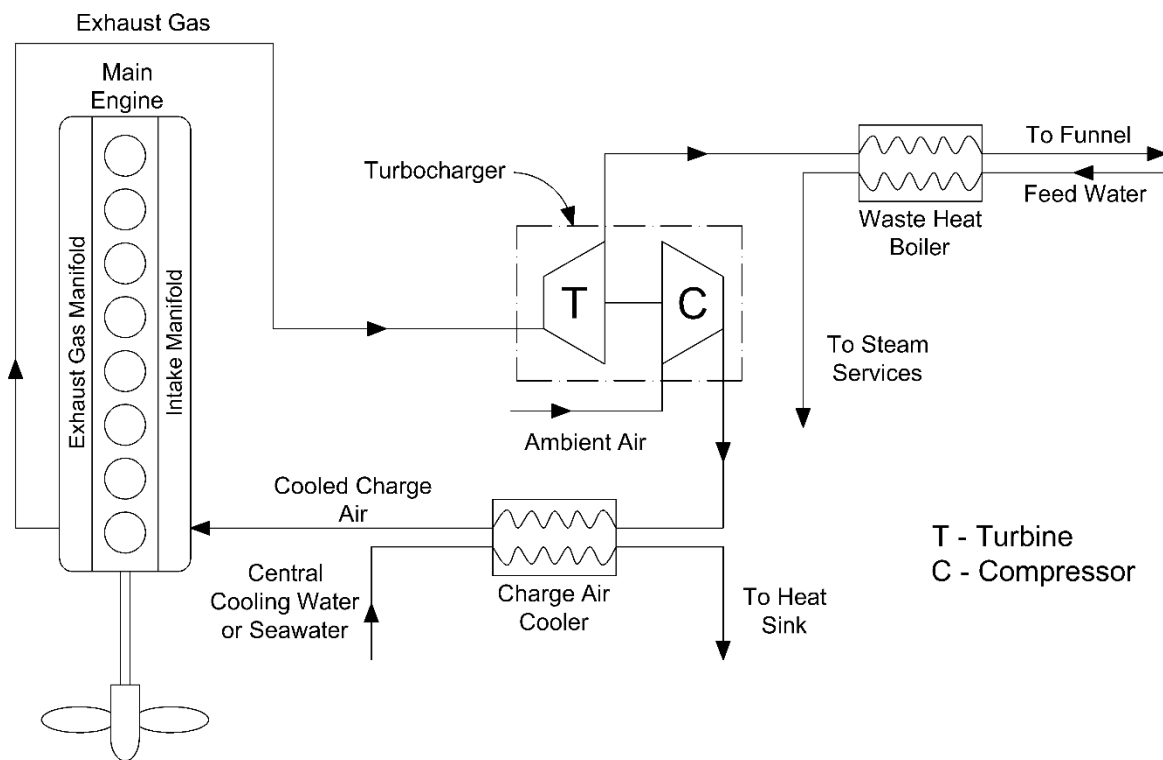


Figure 1. A common marine main engine layout using a charge air cooler and a WHB.

The cold Arctic air represents an opportunity for reduced heat sink temperatures and increased WHRS efficiencies. Drawbacks are large air mass flow rates, fan power input and heat transfer areas due to air low heat transfer coefficient and specific heat [12]. There exists potential to reduce the fan power consumption by using the ship forward movement and passive ventilation designs, as seen in land-based buildings and road vehicles [26,27]. Gil-Baez et al. [28] performed an experimental test on two

buildings comparing the effectiveness of air renewal between mechanical and natural ventilation strategies. The authors demonstrated that by using natural ventilation strategies, between 18-33% of energy could potentially be saved. Hiyama and Glicksman [29] studied the target air change rate for natural ventilation where occupant thermal comfort is starting to reach its maximum value. This approach supports early-design stages to optimise energy performance and cost-effectiveness of projects. Medved et al. [30] proposed a numerical algorithm for optimisation of free-cooling system with night ventilation. The authors considered a weather predicted control to achieve highest possible efficiency proving the energy performance advantages of natural ventilation over mechanical strategies (despite the constraint on air exchange rate due to the use of a passive system).

Considering the various approaches to passive ventilation when applied to ORC applications, the simplest approach is to arrange the heat exchangers on the open deck. This is not uncommon for land-based cooling in thermal power plants and air conditioning, where ground or roof space is available (Figure 2A). However, in the marine application, the attractiveness of this concept is limited by; the need to handle a wide range of apparent wind directions; the additional maintenance load involved in supporting exposed upper deck equipment; competition for upper deck space (and interference with other activities); and the subsequent location of the heat exchangers in the decelerated and turbulent flow close to the deck, which may reduce the air flow rates. Cooling towers may occupy less deck space, but have limitations; for example, Wang et al. [31] investigated the cooling performance of a natural draft cooling tower at various wind speeds using Computational Fluid Dynamics modelling. The authors demonstrated that in order to increase ventilation rates by 36% at high wind speeds when crosswind is present, a windward opening was necessary. Windscoops can rotate into the wind (Figure 2B) and is an established method [32] of increasing ventilation below-decks on ships and in low-energy buildings. Being raised above the deck, they may experience higher wind speeds, but do necessitate long ducts, with multiple changes in direction, causing frictional losses and reducing performance.

More sophisticated wind catchers and wind towers (Figure 2C) can use the pressure differential on the windward and leeward sides of a structure to generate an internal airflow. These have seen extensive use in land based applications, with the aim of exploiting ambient wind conditions to drive building ventilation. These can also be combined with thermal systems using the chimney or stack effect – where warm internal air rises up a chimney, so creating a natural draft [33]. Appropriately shaped devices can use external airflow to increase the updraft in chimneys (Figure 2D). These can take the form of Venturi-shaped devices, which cause significant reductions in the local air pressure over the top of the chimney or ventilation stack, so increasing draft [34]. Again, these can be combined with other techniques and are being investigated for use in low-energy buildings.

The aim of this paper is to investigate the reduction of the parasitic fan power requirements of an air-cooled condenser for a marine ORC unit by using the ship forward movement and passive ventilation approaches. This is the first paper considering the performance improvement of an air-cooled marine

ORC-based WHRS by means of air flows produced by the ship forward moment and passive ventilation techniques. The paper contributes to the literature of air-cooled WHRS for commercial shipping, ship design and ventilation by studying the benefits of reducing the ship CO₂ emissions by using alternative cooling approaches for the marine WHRS in extremely cold weather. The paper sets in section 2 the case study for this work. Section 3 outlines the method used and section 4 presents the results achieved by the different cooling approaches for the ship ORC unit. Section 5 discusses the limitations of the analysis carried out, assumptions made and possible future research routes for exploring the proposed cooling system, and finally, the main conclusions are outlined.

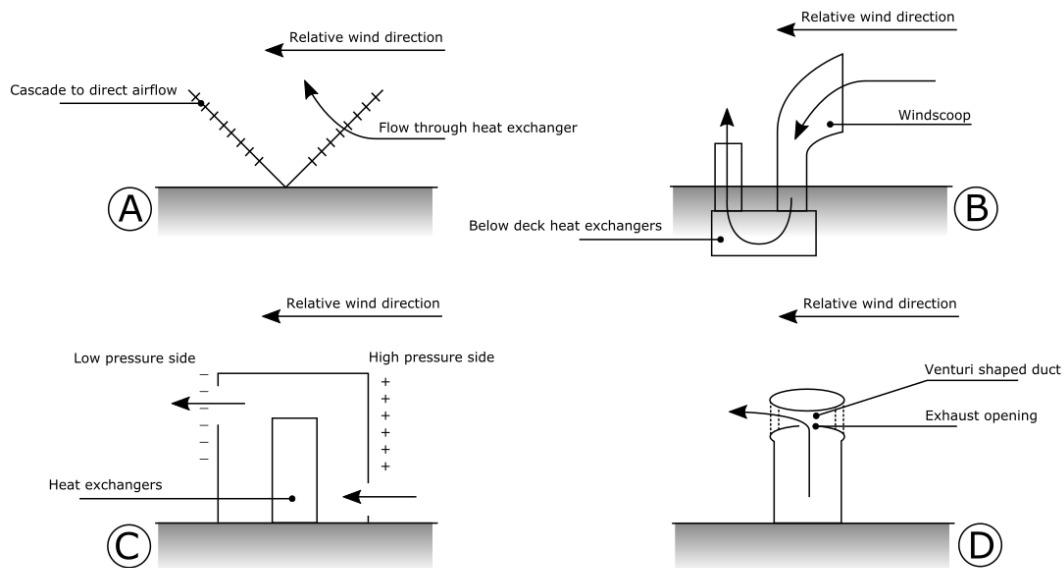


Figure 2. Four possible options for using apparent airflow to cool the ORC unit condenser.

2. Case Study

At present little detailed data is available for merchant ships that take the polar route from Asia to Europe and hence the case study presented here will consider a vessel operating in the low Arctic sailing between northern Norway and Iceland.

2.1 The ship

A hypothetical 4,130 twenty-foot equivalent unit (TEU) containership is used to study the performance of the WHRS and its power demand when sailing in the Arctic [35,36]. The propulsive power is calculated using UCL's Whole Ship Model with the ship characteristics described in Suárez de la Fuente et al. [21]. The operational profile, shown in Table 1, was obtained using anonymised Automatic Identification System (AIS) data from containerships navigating in the Arctic during 2012 provided by UCL's Energy Institute. Note that there is no impact of sea state.

Table 1. Operating profile for the hypothetical containership.

Speed (kn)	Power Required (kW)	Rating (% Maximum Continuous Rating)	Time (%)	Scavenge Air Temperature (°C)	Scavenge Mass Flow Rate (kg/s)
<19.8	<16,810	<41	47.4	79	39.6
21.0	20,925	51	20.3	98	44.9
22.1	25,210	61	15.5	118	55.6
23.3	30,844*	75	12.8	140	76.0
24.6	37,550	91	4.0	160	86.8

* Design point

To reach a maximum speed of 25.2 knots, a 41,125 kW two-stroke low-speed Diesel engine is used [37]. The main and auxiliary engines consume HFO with an assumed Carbon Factor of 3.1144 g CO₂/g fuel [38]. The on board electric demand, while at sea, is assumed constant at 1,390 kW_e [38] with an auxiliary engine specific fuel consumption (SFC) of 227 g/kWh at 85% Maximum Continuous Rating (MCR).

2.2 Route characteristics

The 1,980 km route starts from Reykjavik, Iceland and ends in Ballstad, Norway, with an assumed 4.3 round trips per month [21] equivalent to 54 sailing hours per single trip. The annual CO₂ emissions for the base ship is 59,600 t, of which 54,000 t are produced by the main engine and 5,600 t by the auxiliary machinery. The ambient air temperatures, from the CRUTEM4 data set [39,40], are shown in Table 2.

Table 2. Monthly ambient air temperature seen on the studied route.

	Jan	Feb	Mar	Apr	May	Jun	Jul	Aug	Sep	Oct	Nov	Dec
Air Temperature (°C)	-1.7	-1.1	-0.9	1.0	4.0	5.4	7.3	7.3	7.4	4.1	1.4	-0.5

For the wind data, the route is discretised into 44 waypoints. A random voyage date is chosen and for each waypoint along the route the wind data [41] for that date and time is polled. This process is repeated 500 times to have sufficient results to represent the entire 36-year period for which data is available. The resultant data is clustered from which probability distributions are obtained (see Table 3) for each True Wind Speed (TWS) and True Wind Angle (TWA). The TWS is defined as the wind speed measured from a stationary position while True Wind Direction (TWD) is the wind angle (Γ) relative to the true north (i.e. the geodetic north) experienced at the same stationary position (see Figure 3). The TWD has been converted, using the ship route, to TWA which refers to the wind angle in relation to the ship bow or heading. It goes from 0° – wind on the bow – to 180° – wind on the stern, and when TWA is 90° it means a wind on the beam.

Table 3. Probability distribution for true wind speed (TWS) and true wind angle (TWA) seen from the ship bow along the route.

TWS (m/s) \ TWA (°)	0	2	4	6	8	10	12	14
0	0.00%	1.26%	0.21%	0.42%	0.00%	0.00%	0.00%	0.00%
45	1.26%	5.03%	6.92%	2.10%	1.89%	0.00%	0.00%	0.00%
90	0.21%	7.34%	12.58%	7.13%	7.55%	2.10%	0.00%	0.00%
135	0.84%	6.71%	10.69%	5.24%	3.98%	1.89%	0.84%	0.63%
180	0.21%	3.14%	4.61%	2.31%	1.26%	1.05%	0.42%	0.21%

The combination of the forward motion of the ship and true wind velocity will lead to an apparent wind velocity as seen from on board the ship, as illustrated in Figure 3.

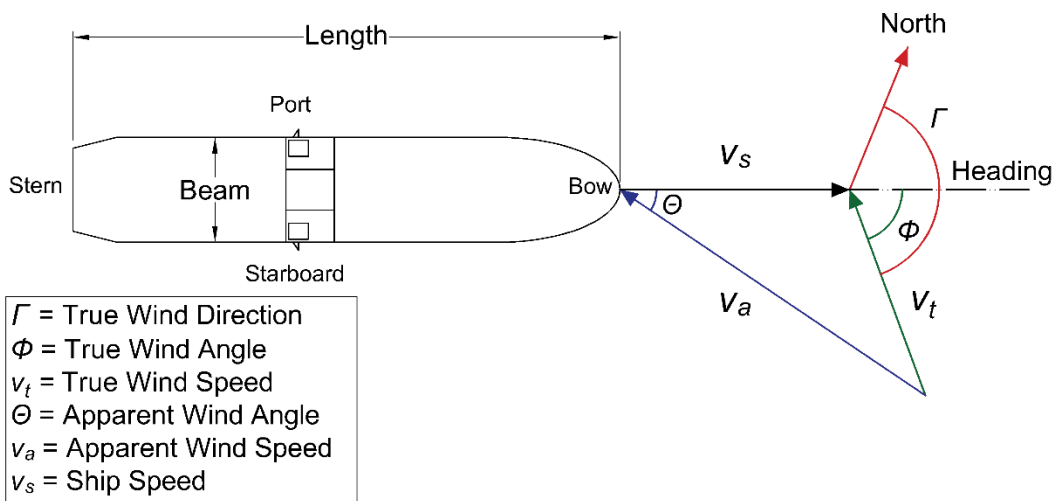


Figure 3. Depiction on the true and apparent wind vectors acting on the containership.

This will not be experienced uniformly over all relative headings, as shown in the data published by the Ship Structure Committee [42]. The data on Table 3 was transformed to Apparent Wind Speed (AWS) and Angle (AWA) depending on the ship velocity and heading. Using Figure 3, the hypothetical ship is navigating with a velocity vector v_s at a speed of v_s in the bow direction (i.e. the heading) while the true wind vector v_t arrives at the ship bow at a speed v_t (i.e. TWS) and with an angle ϕ (i.e. TWA). Solving for the vectors, it is possible to find the apparent wind vector v_a , which is formed by the AWS v_a and AWA θ [43].

2.3 Waste heat recovery system

For this study the charge air temperatures are partly reduced via the ORC unit once-through boiler rather than the air cooler [37]. The waste heat absorbed by the boiler is used to generate electrical power via the ORC unit thermodynamic processes and an electrical generator (see Figure 4). The electrical power produced is supplied to the ship's grid which in turn will have an impact on the auxiliary system loading and specific fuel oil consumption with the aim of reducing fuel consumption and CO₂

its application in marine WHRS as it combines the air flow caused by stack effect, ship forward movement and natural wind speed, and forced air due to the fan.

The concept uses two windscoops with a capture area of 2 m² each and they are positioned at either side of the ship superstructure (Figure 5). The windscoops are capable of rotating on their own axis perpendicular to the ship superstructure in order to capture the wind component in the upwind and downwind direction. The windscoop design idea is taken from the rotating ducted thrusters used in hovercrafts for manoeuvring [49]. A limitation of this design is that it only captures the apparent wind speed component in the longitudinal direction and not capturing the beam or side wind speed component. The chimneys are integrated into the superstructure to minimise structural weight and wind drag. The chimney exhaust is assumed to be one deck, 2.8 m, above the bridge and having a superstructure with six decks, the chimney exhaust is 19.6 m above the upper deck. The chimney diameter is assumed to be 2 m. The ship beam (width) is the same as the superstructure beam, at 32.2 m. The Venturi-shaped roof is of an omnidirectional construction with no guiding vanes which gives the highest pressure coefficients at different wind angles [34]. The Venturi-shaped roof has a contraction ratio of two with a flow area on top of the chimney exhaust of 2 m². The design optimisation of windscoops and other passive ventilation equipment are outside the scope of this work but it is an interesting area for further developments.

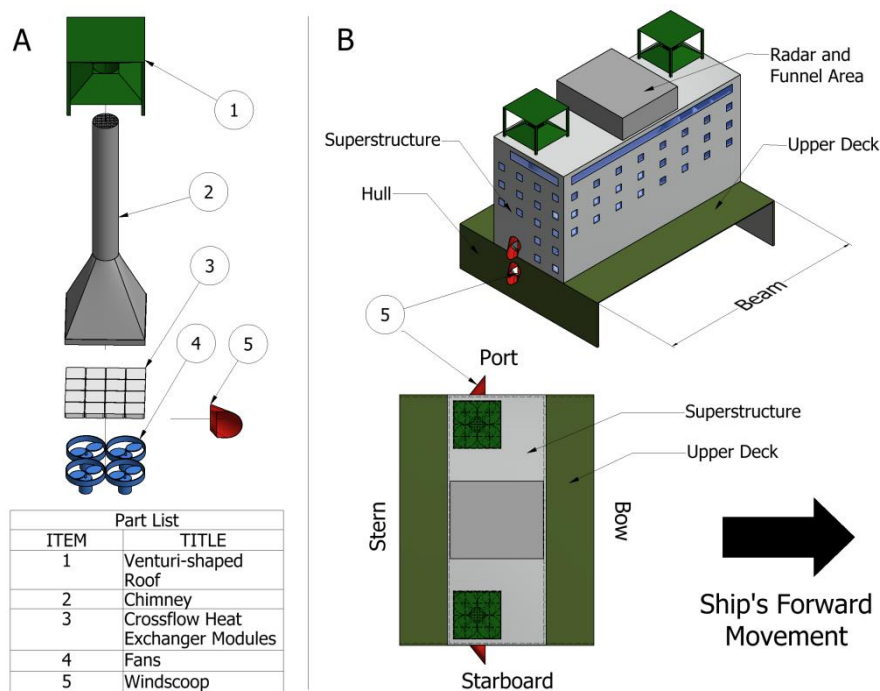


Figure 5. A) Hybrid cooling system components for the ORC unit. B) Suggested location for the ORC unit cooling system with different parts of the ship as well as the direction of the ship movement.

It is important to mention that the hybrid cooling system has a supportive role in covering the air flow demand for the ORC unit and it is not intended as a substitute of the condenser's fan.

3. Method

3.1 Waste heat recovery system

For the ORC unit a simple layout was chosen for this study and it is formed of a boiler, expander, air condenser and pump (Figure 6). The simple layout is an attractive option when there is a relatively low temperature at the waste heat source because the benefit of a recuperator (i.e. higher ORC unit thermal efficiency and power output) is minimal but the cost penalty is still present [10,22,50]. Furthermore, machinery rooms on board ships tend to be tight and compact systems are desirable. As mentioned by Sellers [51] the system compactness is even more important in retro-fit applications where the machinery layout cannot be modified easily, cheaply and without the need to recertify equipment. This section describes the ORC unit modelling without the implications of passive cooling while section 3.2 deals with the passive cooling modelling and its implications on reducing the ORC unit ancillary demands.

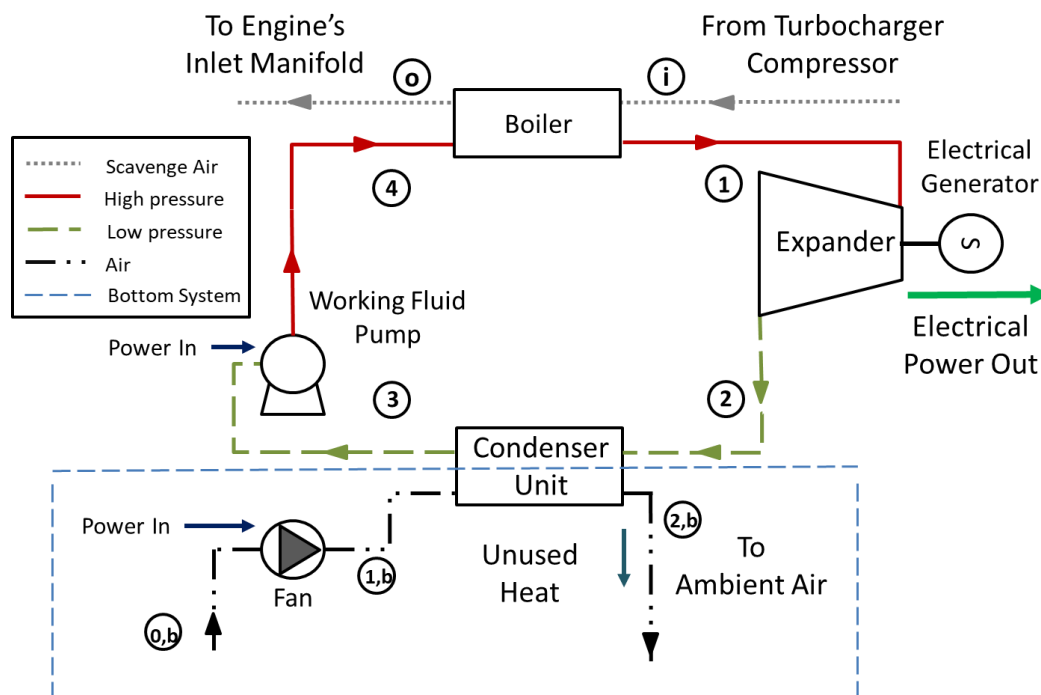


Figure 6. Organic Rankine Cycle unit layout using the waste heat available in the scavenge air system and rejecting the excess heat to the ambient air.

The optimisation of the 13-dimensional space was carried out using a single objective approach using Particle Swarm and Pattern Search algorithms [12]. Table 4 presents the ranges for the independent variables used to optimise the ORC unit design. The number of variables allow the simulation to explore a large sample of possible ORC unit and air condenser designs and find the best solution for the studied container ship. In particular, the three pressure points, selected by the optimisation algorithm were used to produce a spline interpolation curve that governed the ORC off-design evaporation pressures. The off-design strategy, in terms of pressures, was thus optimised rather than presumed. Thermodynamic

and numerical checks (e.g. energy balance and pump flow direction) were added to the optimisation process with the purpose of eliminating design solutions that do not follow the thermodynamic laws.

Table 4: Optimisation independent variables and their ranges explored for the design definition of the ORC and air condenser units.

Parameter	Range	Used for
Scavenge Air Outlet Temperature (°C)	50 - 120	ORC unit
P_1 (kPa)	300 – 3,440	ORC unit
$P_{1,off1}$ (kPa)	$(0.50 - 1.00) \cdot P_1$	ORC unit
$P_{1,off2}$ (kPa)	$(0.35 - 1.00) \cdot P_1$	ORC unit
$P_{1,off3}$ (kPa)	$(0.20 - 1.00) \cdot P_1$	ORC unit
Superheating Temperature (°C)	5 – 100	ORC unit
Condenser Unit Pinch Point Temperature Difference (°C)	5 – 25	ORC unit and Condenser unit
WHRS Design Point (Ship Speeds)	75% -105% of Design Speed (27% - 91% MCR)	ORC unit
Tube Internal Diameter (mm)	16 – 100	Condenser unit
Tube length (m)	1.83 – 7.32	Condenser unit
Fin Height (mm)	2 – 16	Condenser unit
Fin Thickness (mm)	$8 \times 10^{-2} - 25 \times 10^{-2}$	Condenser unit
Fin Pitch (mm)	2 – 24	Condenser unit

As mentioned before, the ORC unit boiler substitutes the air cooler as the equipment to cool down the scavenge air. Using Figure 6, the hot charged air enters the ORC unit where the air temperature is reduced while heat extracted is transferred to the refrigerant (4-1). The waste heat transferred to the refrigerant (\dot{Q}_{WH}) was calculated as follows:

$$\dot{Q}_{WH} = \dot{m}_{WH} \cdot c_{p,WH} \cdot (T_i - T_o) \quad (1)$$

Where \dot{m}_{WH} is the mass flowrate and $c_{p,WH}$ is the scavenge air specific heat, T_i and T_o are the scavenge air inlet and outlet temperature respectively. The \dot{m}_{WH} at the different operating points were taken from

[37], while T_o and the design point for the ORC unit were chosen by the optimisation process. Noting that adding heat or work to the system has a positive sign while a negative sign is used to signify heat or work extracted from the system. The pressure losses due to the ORC unit's boiler at different operating conditions are assumed to be the same as those experienced with an air cooler which are between 1.0 kPa and 3.5 kPa [52], small enough to neglect their effect on the main engine performance [53]. A detailed study of the ORC unit once-through boiler design is out of the scope of this work but the interested reader can consult reference [54].

The condenser unit (2-3) has the task of rejecting the ORC unit excess heat to the sink which in this case is the ambient air found in the Arctic. It is assumed that at the condenser exit the working fluid will be at its liquid saturated condition with a fixed temperature of 25°C. The heat rejected to the heat sink (\dot{Q}_{co}) is given by:

$$\dot{Q}_{co} = \dot{m}_{wf} \cdot (h_3 - h_2) \quad (2)$$

Where \dot{m}_{wf} the working fluid mass flow rate, and h_2 and h_3 are the specific enthalpies before and after the heat rejection process; the calculation of these variables will be discussed later in this section. The advantage of having a relatively high saturation temperature – in comparison to ambient air found in the Arctic – is that the ORC unit can operate the whole year in the proposed Arctic route (see Table 2) with a wide range of possible pinch points allowing for lower coolant mass flow rates and fan power consumption. A side effect of this design decision is that fixing the saturation temperature at a higher point constrains the expander power output by not taking advantage of the larger expansion given by lower ambient air temperatures. However, as shown in Suárez de la Fuente [21], the power requirement from an air-cooled ORC unit fan can increase considerably with a small change in the ambient air temperature. Under these fixed conditions at the exit of the condenser unit it is possible to find P_3 and h_3 . The ORC unit high pressure (P_1 and P_4 are the same due to the no pressure losses assumption at the boiler) is selected by the optimisation method from the ranges shown in Table 4.

Turning to the ORC unit pump, the working fluid specific enthalpy after the pump (h_4) was found as follows:

$$h_4 = h_3 + \frac{(h_{4s} - h_3)}{\eta_p} \quad (3)$$

Where h_{4s} is the specific enthalpy after the pump assuming an isentropic increase of pressure from P_3 to P_4 (i.e. P_1) and η_p is the pump's isentropic efficiency assumed to be 80% at design point [55–57]. The off-design pump efficiency (η_p) was modelled to be dependent on the off-design volumetric flow. Pump characteristics from a commercial pump was emulated by accordingly adjusting the coefficients a - d in the following equation, as shown by Larsen et al. [58]:

$$\frac{\eta_p}{\eta_{p,d}} = a \cdot \left(\frac{\dot{V}}{\dot{V}_d}\right)^3 + b \cdot \left(\frac{\dot{V}}{\dot{V}_d}\right)^2 + c \cdot \frac{\dot{V}}{\dot{V}_d} + d \quad (4)$$

Here \dot{V} is volumetric flow and subscript d is short for design point. The working fluid mass flow rate (\dot{m}_{wf}) was given by:

$$\dot{m}_{wf} = \frac{\dot{Q}_{WH}}{(h_1 - h_4)} \quad (5)$$

Knowing these calculated variables, it is possible to find the pump electric power requirement (\dot{W}_p):

$$\dot{W}_p = \frac{\dot{m}_{wf} \cdot (h_4 - h_3)}{\eta_{p,e}} \quad (6)$$

Where $\eta_{p,e}$ is the pump efficiency to convert electrical power to mechanical power and is considered to be a constant 97% [12]. The superheating temperature is also selected by the optimisation method and knowing P_1 (hence the high-pressure saturation temperature) it is possible to determine T_1 and the working fluid specific enthalpy (h_1). At the ORC unit's turbine (1), the working fluid expands and generates mechanical power. After exiting the turbine, the working fluid will be at state 2 where the pressure is the same as P_3 . The specific enthalpy at state 2 (h_2) is calculated as follow:

$$h_2 = h_1 + \eta_{ex} \cdot (h_{2s} - h_1) \quad (7)$$

Where η_{ex} is the expander isentropic efficiency assumed to be 80% at design point [59], h_{2s} is the isentropic specific enthalpy for the expansion process. The expander electrical power output (\dot{W}_{ex}) was calculated as follows:

$$\dot{W}_{ex} = \eta_g \cdot \dot{m}_{wf} \cdot (h_2 - h_1) \quad (8)$$

The expander shaft is connected to a generator with an assumed constant efficiency (η_g) of 97% [12] and it provides electrical power to the ship's grid. Losses found at the power electronics needed to integrate the ORC unit electrical power to the grid are not considered for this study. At off-design the expander efficiency (η_{ex}) was assumed to behave as according to the work of Schobeiri on axial steam turbines [60]:

$$\frac{\eta_{ex}}{\eta_{ex,d}} = \frac{N}{N_d} \cdot \sqrt{\frac{\Delta h_{ex,d}}{\Delta h_{ex}}} \left(2 - \frac{N}{N_d} \cdot \sqrt{\frac{\Delta h_{ex,d}}{\Delta h_{ex}}} \right) \quad (9)$$

Where Δh_{ex} is the enthalpy change during the expansion ratio and N is the expander rotational speed. In addition, the pressures, temperatures and mass flows of the turbine at off-design conditions were related by the Stodola law of the ellipse [61]:

$$C_T = \frac{\dot{m}\sqrt{T_i}}{\sqrt{P_i^2 - P_o^2}} \quad (10)$$

Where C_T is the expander constant and subscripts i and o are short in inlet and outlet of the turbine. Moving to the bottom side of the air condenser unit, the mass flow rate of air required (\dot{m}_b) to absorb the excess waste heat was as follows:

$$\dot{m}_b = \frac{\dot{Q}_{co}}{(h_{2,b} - h_{1,b})} \quad (11)$$

Where $h_{1,b}$ and $h_{2,b}$ is the specific enthalpy before and after the cooling fluid has passed through the condenser unit. Using the condenser pinch point temperature ($\Delta T_{pp,b}$), \dot{Q}_{co} and the air inlet temperature ($T_{1,b}$) is possible to find $h_{2,b}$. To find $h_{1,b}$, the same approach as the one described in equation (3) is used:

$$h_{1,b} = h_{0,b} + \frac{(h_{1s,b} - h_{0,b})}{\eta_f} \quad (12)$$

Where $h_{0,b}$ is the specific enthalpy at ambient air conditions, $h_{1s,b}$ is the specific enthalpy for an isentropic process through the fan and η_f is the isentropic efficiency assumed to be a constant 60% [55]. The electric power required to move the cooling fluid through the condenser unit (\dot{W}_b), assuming that there is no passive ventilation assistance, can be calculated as follows:

$$\dot{W}_b = \frac{\dot{m}_b \cdot (h_{1,b} - h_{0,b})}{\eta_{f,e}} \quad (13)$$

Where $\eta_{f,e}$ is the fan's efficiency to convert electrical power to mechanical power and is considered to be a constant value at 97% [12]. The integration of ship design, route conditions and how the ship is operated has an impact on finding which ORC unit design is the best fit. This has been highlighted in Suárez de la Fuente et al. [62] and more recently by Shu et al. [23]. The models of both the WHRS and condenser unit were optimised to reduce the annual CO₂ emissions using the operating profile shown in Table 1 and weather conditions in Tables 2 and 3 for a whole year. In order to quantify the annual CO₂ savings (CS) achieved by the marine WHRS producing electricity the following equation was used:

$$CS = \frac{C_F \cdot MT \cdot \sum_{i=0}^{OS} \sum_{j=0}^{OM} \dot{W}_{T,WHRS}(i,j) \cdot SFOC_{aux}(i,j) \cdot t(i,j)}{10^6} \quad (14)$$

Where C_F is the fuel carbon factor assumed to be a constant 3.1144 t CO₂ per t HFO [63], MT refers to the monthly single trips, OS are the number of operating speeds as shown in Table 1, OM is the number of months, $\dot{W}_{T,WHRS}$ is the ORC unit net electrical power output given by the addition of \dot{W}_{ex} , \dot{W}_p and \dot{W}_b .

The auxiliary engine fuel is given by $SFOC_{aux}$ in g/kWh and t is the hours spent at each operating speed during the year.

A detailed description of the ORC unit thermodynamic and heat exchanger models with their relevant variables are provided in the following references [21,64–66]. The model was coded in Matlab® 2015a using CoolProp 5.0 [67] package for the working fluid equations of state.

3.2 Passive cooling approaches

The data obtained from the optimisation was post-processed to include the effects of wind speed, angle and air temperature and its contribution to the condenser's fan power reduction. The probability of finding a wind with certain angle and speed as shown in Table 3 is assigned to any given operating speed and month. This means that any operating condition will experience, at some time, all wind conditions.

The volumetric air flow rate produced by the wind captured (\dot{V}_{ws}) by the windscoops is given as follows [68]:

$$\dot{V}_{ws} = C_{ws} \cdot A_{ws} \cdot v_{a,l} \quad (15)$$

Where C_{ws} is the opening effectiveness – how effective the opening is at capturing the wind flow – assumed to be 0.55 which is an intermediate value for perpendicular winds to the windscoop opening [69], A_{ws} is the windscoop opening area assumed to be 2.0 m² and $v_{a,l}$ is the apparent wind velocity component in the ship length direction. In specific to the windscoops, when the total passive flow rate is above the required, the wind cooling will be limited by rotating the windscoops to less favourable angles. For the stack flow (\dot{V}_s) coming from a single chimney is given by the following expression [68]:

$$\dot{V}_s = C_D \cdot A_{ch} \cdot \sqrt{\frac{2 \cdot g \cdot \Delta H_{NPL} (T_{2,b} - T_{amb})}{T_{2,b}}} \quad (16)$$

Where A_{ch} is chimney outlet cross-sectional area, g is acceleration due to gravity and assumed to be 9.81 m/s², ΔH_{NPL} is the height from the midpoint of lower opening to neutral pressure level assumed to be 0.25 m above the chimney exit (i.e. 19.85 m), T_{amb} is the ambient air temperature and C_D is the discharge coefficient assumed to be the same for both openings and it is given by [68]:

$$C_D = 0.40 + 0.0045 \cdot |T_i - T_{amb}| \quad (17)$$

The pressure drop found at the middle of the chimney generated by the Venturi-shaped roof is found using the Bernoulli equation. This gives a pressure coefficient (C_p) of -0.75, which is a conservative value [34,70], and it is assumed to be the same for any wind angle due to the omnidirectional nature of the roof. The flow rate due to the Venturi-shaped roof (\dot{V}_{vr}), found the same way as an intentional opening, to the flow is then calculated as follows [68]:

$$\dot{V}_{vr} = C_D \cdot A_{ch} \cdot (v_{vr} - v_a) \cdot \sqrt{|C_p|} \quad (18)$$

Where v_{vr} is the air speed at the chimney centre accelerated by the Venturi-shaped roof contraction, assuming there is no air leakages or changes in height, and v_a is the magnitude of the apparent velocity vector \mathbf{v}_a . The total air volume flow rate (\dot{V}_T) going through the condenser is calculated with the quadrature superposition method which gives a good approximation for the total flow when compared to other empirical methods [71]. The air flow supplied to the heat exchanger is given by the following approximation [68,71]:

$$\dot{V}_T = \sqrt{\dot{V}_f^2 + \dot{V}_{ws}^2 + \dot{V}_S^2 + \dot{V}_{vr}^2} = \dot{m}_b / \rho_{amb} \quad (19)$$

Where \dot{V}_f is the fan flow rate required and $\rho_{1,b}$ is the air density at atmospheric conditions. In the case of twin chimneys design, as shown in Figure 5B, it is assumed that when the wind is captured at the port side then at starboard the wind pressure will be negative (see Figure 2) and wind will be blocked for the Venturi-shape roof to enhance the warm air suction. Under these circumstances only the fan and stack flow rates will be operating. The power reduction due to the use of passive cooling was evaluated by finding the proportional contribution of each of the passive cooling methods with respect to \dot{V}_T and then multiplying it to the condenser total power requirement. This is represented in Equation (17), to calculate the electrical power reduction using the windscoops (\dot{W}_{ws}):

$$\dot{W}_{ws} = \dot{W}_b \cdot \frac{\dot{V}_{ws}}{\dot{V}_T} \quad (20)$$

Having the participation of the different passive cooling systems it is possible to find the electrical load for the condenser's fan (\dot{W}_f):

$$\dot{W}_f = \dot{W}_b - (\dot{W}_{ws} + \dot{W}_S + \dot{W}_{vr}) \quad (21)$$

Where \dot{W}_S is the electrical power reduction coming from the stack flow and \dot{W}_{vr} is the electrical power reduction produced by the Venturi-shaped roof. In order to evaluate the monthly passive cooling contribution to the ship, the electrical power was changed to energy. The energy calculation for the windscoops' cooling (E_{ws}) in electric kilowatt per hour is given as follows:

$$E_{ws} = \sum_{i=0}^{OS} \sum_{j=0}^{OM} \sum_{k=0}^{OW} \dot{W}_{ws}(i, j, k) \cdot t(i, j, k) \quad (22)$$

Where OW represents the wind conditions shown in Table 3 and t is the time, in hours, spent at each operating ship speed under the different wind speeds and angles during the whole year. The same method is used for the total energy required at the condenser unit and the other ORC unit's passive cooling systems analysed in this work.

Pressure losses due to ducting and flow through the chimney were assumed insignificant. The implications of fan locations, ducting path and the energetic cost, drag and movement, of the rotating windscoops and Venturi-shaped roof is beyond the scope of this work.

3.3 Model validation

The WHRS thermodynamic model was used in Larsen et al. [64]. There was a 1% difference on the heat exchanger overall heat transfer coefficient when compared to Richardson and Peacock [72]. The air condenser model gave an error of 0.3% and 0.5% for the logarithmic temperature difference and the outlet temperature respectively when compared to Gnielinski [73]. The wind and stack flows were validated against results of EnergyPlus™. For a headwind of 11.4 m/s, at a temperature of -25.3°C with a TWA of 30° and a rejection of 1650 kW there is a fan power reduction of about 32.7% while when using it EnergyPlus™ the reduction was 28.5%. The difference could be caused by the chimney and duct frictional losses not considered in this work.

4. Results

4.1 Organic Rankine cycle unit

The ORC unit, with its condenser design and performance as shown in Tables 5 and 6, is capable of reducing the CO₂ emissions by 543 t/year without the hybrid cooling which represent 0.91% of the annual container ship CO₂ emissions and 9.70% of the annual CO₂ emissions produced by the auxiliary machinery. The ORC unit operates when the ship speed is 21.0 knots and above which represents 52.6% of the navigational time. Below this engine load the waste heat temperature is lower than 100°C where the ORC unit does not generate electric power.

Table 5. Some of the design characteristics for the hybrid cooling approach for a single chimney. The air requirement and cooling loads are given for design speed and ambient air temperature of 7.4°C.

Modules (-)	Length (m)	Width (m)	Tube rows (-)	Frontal Area (m ²)	Heat Rejected (kW)	Air Requirement (m ³ /s)
43	7.30	6.34	5	46.30	1648.5	87.4

Table 6. Some of the performance characteristics for the ORC unit condenser for a single chimney split in the section where the organic fluid is being cool down to its saturated vapour condition (desuperheating section) and where the organic fluid condensate (condensing section) . The heat transfer coefficients are given for design speed and ambient air temperature of 7.4°C. The surface area quantities includes tubes and their fins.

P₃ (kPa)	Condensing Section			Desuperheating Section		
	Surface Area (m ²)	Overall Heat Transfer Coefficient (W/m ² ·K)	UA (W/K)	Surface Area (m ²)	Overall Heat Transfer Coefficient (W/m ² ·K)	UA (W/K)
129.3	6,203	16.9	326.3	2,298	5.4	104.7

During the summer when the air temperatures are high, a maximum fan consumption of 25 kW_e is seen at design speed (i.e. 23.3 knots) which results in the lowest ORC unit net power (see Figure 7). Looking

at the different ship speeds, it is possible to see that as the ship speed increases the larger it is the net electric power output produced by the ORC unit (Figure 8A). The maximum net power output, 451 kW_e, is achieved when the operational speed is 24.6 knots and the ambient temperature is the lowest (i.e. -1.7°C in January). Under this scenario, the scavenge air mass flow rate and temperature at the entrance of the ORC unit boiler is higher, allowing for a larger waste heat absorption. As the ship speed is reduced, the scavenge air temperature drops and the cooled air flow requirement to the engine becomes smaller, causing, in January, a drop in the ORC unit power output of about 61% or 277 kW_e. The fan power requirement during the whole year at the different operational speeds when the ORC unit is working can be seen in Figure 8B.

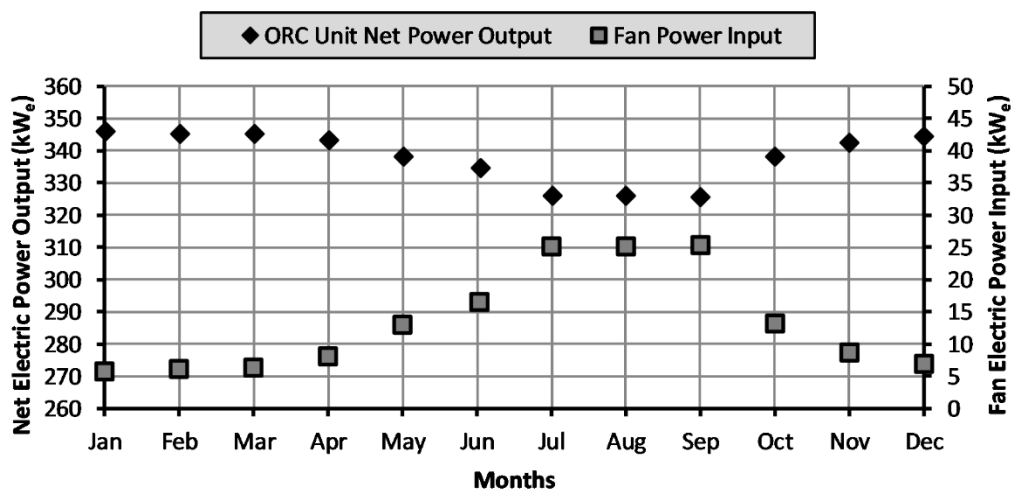


Figure 7. Monthly ORC unit net electric power output (right) and fan electric input (left) at ship design speed (i.e. 23.3 knots), no passive cooling power included.

For all operational speeds it can be appreciated that the ambient air temperature has an effect on the fan power demand as discussed previously. However, at the lowest speeds the power demanded increases from winter to summer is lower than at the fastest speeds. At 24.6 knots, the fan power input in January is about 10 kW_e and in September increases to about 49 kW_e, while at 21.0 knots the fan power input over the same period increases from 2 kW_e to 10 kW_e. For this reason, the net electric power through the year, Figure 8A, for the slowest operational speeds (i.e. 21.0 and 22.1 knots) is relatively stable.

The energy analysis of the ORC unit's fan for a single trip shows that the maximum energy demand happens in September at 501 kWh_e while the lowest is found in January at 113 kWh_e (Figure 9). The annual fan energy demand represents about 6.2 t of fuel and 19.2 t of CO₂, which represents 3.5% of the net annual CO₂ savings achieved by the ORC unit.

4.2 Hybrid cooling

Due to the fluctuation in apparent wind caused by the multiple combinations of headings, ship operational speeds, true wind speeds and angles, the reduction in fan power demand caused by the

proposed hybrid cooling system changes. This is highlighted by Figures 10A and 10B for the starboard hybrid system when the ship is navigating at design speed in January and September respectively, which are the extreme cases for minimum and maximum fan energy demand as per Figure 9. The performance of the port system will be a mirror of Figure 10. From Figure 10A, it can be seen that with headwinds, at design speed, at different wind speeds produce enough flow to cover between 58% and 100% of the condenser electrical power demand. With winds above 10 m/s there is no need to use the fan and due to an excess of air flow, the windscoops are rotated to less favourable angles to balance the cooling flow with the demand. For winds of 0 m/s, the flow is produced solely by the ship forward movement and represents 60% of the fan electric power input, or 1.6 kW_e.

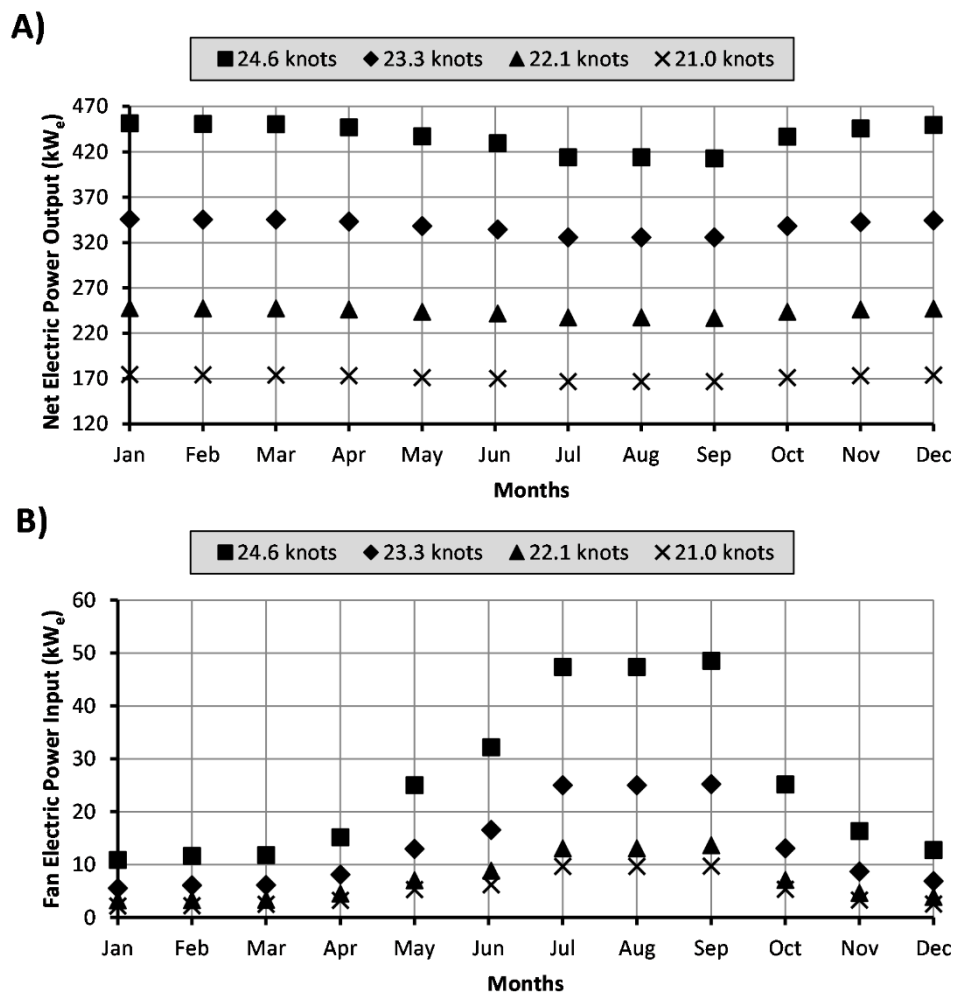


Figure 8. A) Net electric power output generated by the ORC unit at the different ship operational speeds during the year; B) Fan electric power consumption for different speeds and months of the year.

At a TWA of 90°, the assistance of the hybrid system is between 58% to 66% of the cooling flow demand. The Venturi-shaped roof is the equipment that takes the most advantage of the high TWS, changing from a representative 0.6 kW_e with winds of 0 m/s to 0.8 kW_e at 14 m/s. At the same angle, the stack and captured flow from the windscoops remains similar at 0.2 kW_e and 0.9 kW_e respectively.

As the TWA moves to the stern, the benefit of having high TWS at design speed reduces considerably due to the wind speed being similar as the ship's operational speed but in the opposite direction. A wind of 2 m/s represents around 51% of the fan electrical power input while at 12 m/s – or 23.3 knots which is the ship design speed – this drops to about 11%. Under this case only the stack flow is working in conjunction with the fan. This occurs because the cooling performance depends on the apparent wind speed; a combination of TWS and TWD coupled with the ship speed. Thus, when the ship is heading away from the wind, the apparent wind speed is lower and so is the cooling performance. When the wind is being blocked by the ship superstructure (i.e. wind angles between 180° and 360°) only the cooling performances of the stack flow and fan will be operating for the ORC unit condenser.

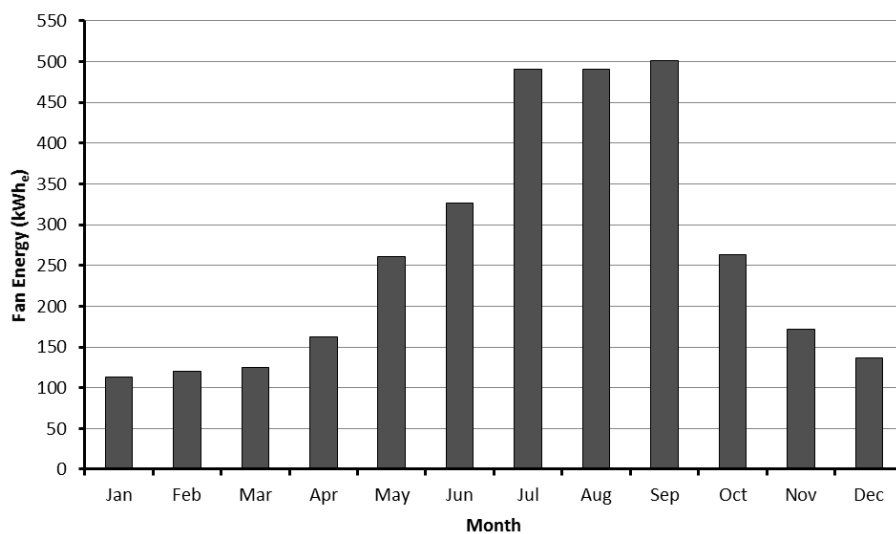


Figure 9. Monthly ORC unit fan energy demand for a single monthly trip.

It can be seen from Figure 10B that the hybrid cooling behaviour in September for different TWS and TWA is similar to that seen in January but is proportionally smaller. The hybrid system represents between 36% to 62% of electrical power demanded for TWS between 0 m/s and 14 m/s when TWA is 0°. When the ship is experiencing tailwinds, the proportional part of the electric demand covered by the hybrid system is smaller, between 5%, at a TWS equal to the ship design speed, and 36% when there is no wind. The reason of the smaller proportional contributions is that the starboard condenser unit power requirement is around 12.6 kW_e, about 4.8 times larger than in January, due to both the increase in ambient air temperature and reduction in density, with associated increased volume flow rates. In January when the average ambient air temperature is -1.7°C, a volumetric flow rate of 30.6 m³/s and a power of 2.8 kW_e is required for the starboard ORC condenser. In September, when the air is warmer at 7.4°C, the volumetric flow rate and power increase to 55.9 m³/s and 12.6 kW_e respectively. Hence the power requirement to move a cubic metre of air in January is 0.09 kW_e/(m³/s) while in September it is 0.22 kW_e/(m³/s).

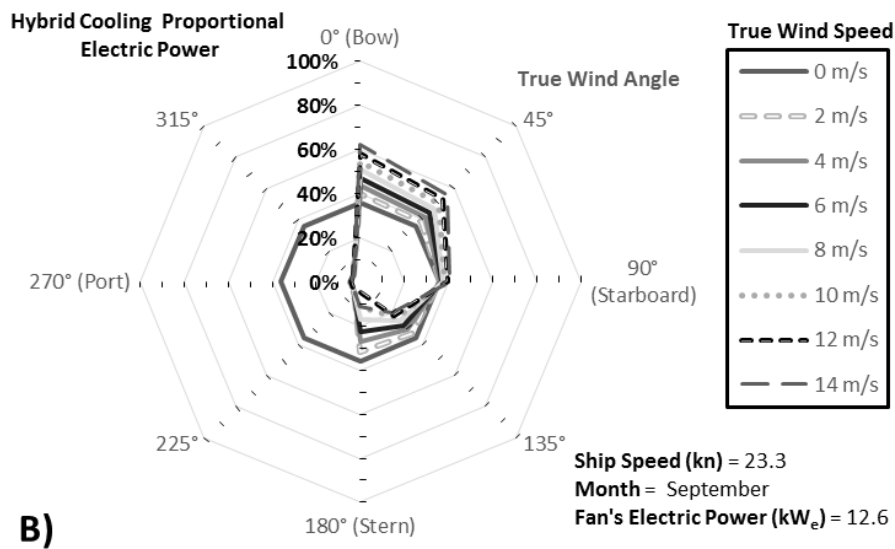
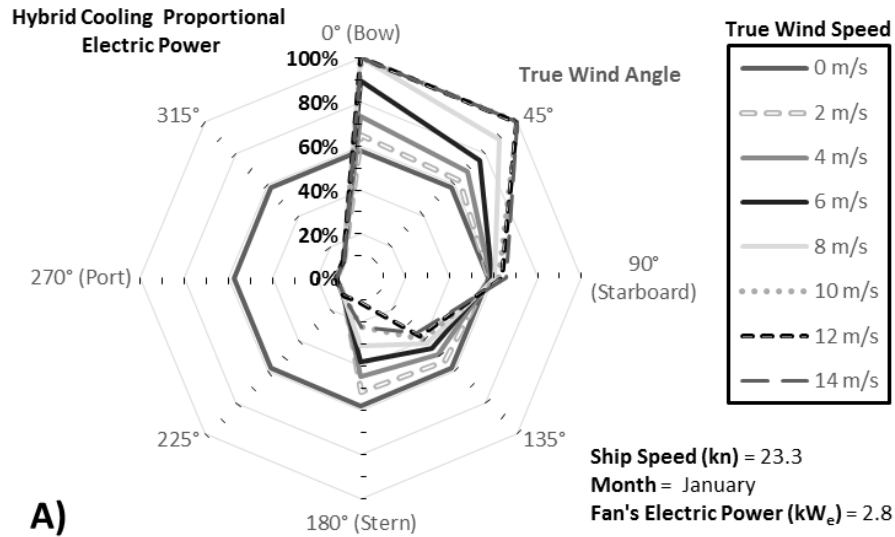


Figure 10. Electric power proportion of the starboard hybrid system to the total condenser unit electric power demand for the month of A) January and B) September when the containership is navigating at design speed.

For other months of the year, a similar hybrid cooling behaviour is seen as in Figures 10A and 10B but with different proportions to the total power demanded which are inside the boundaries established by the months of January and September. In the case of the fastest operational speed, although there is a larger air flow produced by the hybrid system, it has a smaller net impact due the larger overall electrical power demand at the condenser (see Figure 8B). For example, the maximum electrical power substituted by the hybrid cooling for the starboard equipment in September is 12.6 kW_e at a TWS of 14 m/s and a TWA of 0°, which represents about 52% of the total electrical power demand. At the same month and when the system is blocked, it only provides 3.4% of the demanded power. On the other hand, at the slowest speed where the ORC unit is operating, in January, TWS above 2 m/s and TWA between 0° and 45° cover 100% the electric demand at the condenser unit which is 1.1 kW_e.

During the whole year of operation, the twin hybrid cooling system considering the fan power demand reduction while unblocked and blocked saves 1.6 t of fuel and 4.9 t of CO₂, which is a 0.9% increase on saving by the ORC unit. The total CO₂ emission reduction of 548 t of CO₂ with the hybrid cooling represents a reduction of 0.92% of the ship's annual CO₂ emissions and 9.80% of the auxiliary machinery emissions. The low savings are caused mainly by a low probability of encountering favourable winds for passive cooling, such as headwinds of any speed which only amount to about 2% of the total navigational time or about 64 minutes in a single trip (see Table 3 and Figure 11). Other factors are low windscoop and Venturi-shaped roof capture areas with no optimisation for the air flow rates required; and the assumption that when AWA is at any angle on the beam, only one passive system is fully operational. Putting the results into perspective, if the ORC unit condensers were operating only with fans, the fuel consumption due to the condenser cooling is around 6.2 t which means that the passive cooling brings a 26% reduction in condenser cooling electrical load.

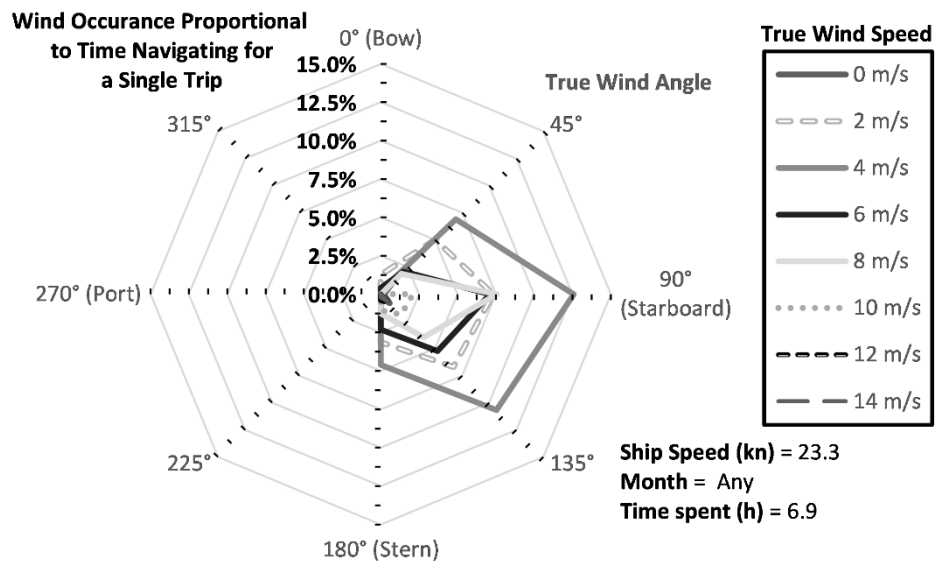


Figure 11: Proportion of time spent at each wind condition for any single trip of the year seen where the starboard hybrid cooling system is unblocked for a ship speed of 23.3 knots.

Examining a single trip with the hybrid system fully operating (i.e. not being blocked by the ship structure or containers), the fuel saving is about 152 kg. The passive system in January substitutes 33.5 kWh_e from the fan and in September it reaches 88.6 kWh_e, see Figure 12. The largest passive cooling contribution is from the windscoops, followed by the Venturi-shaped roof and the stack effect. The stack flow contributes to the net hybrid cooling by 3.6% to 8.1% of the total energy. As the ambient air temperature increases, the stack volumetric flow reduces due to a lower density difference between the ambient air and the air exiting the condenser. The Venturi-shaped roof suffers from the same issue and has a proportional contribution of around 21.1% in January and 12.3% in September. The wind volumetric flow rate stays the same during the different months, but changes with the ship and apparent wind speeds. In September, it supplies 19.5% of the cooling energy requirement and 29.9% in January.

The volumetric flow rate is sensitive to ambient air temperature and for ships that might operate in the high Arctic where ambient temperatures are even lower passive cooling could contribute a significantly more.

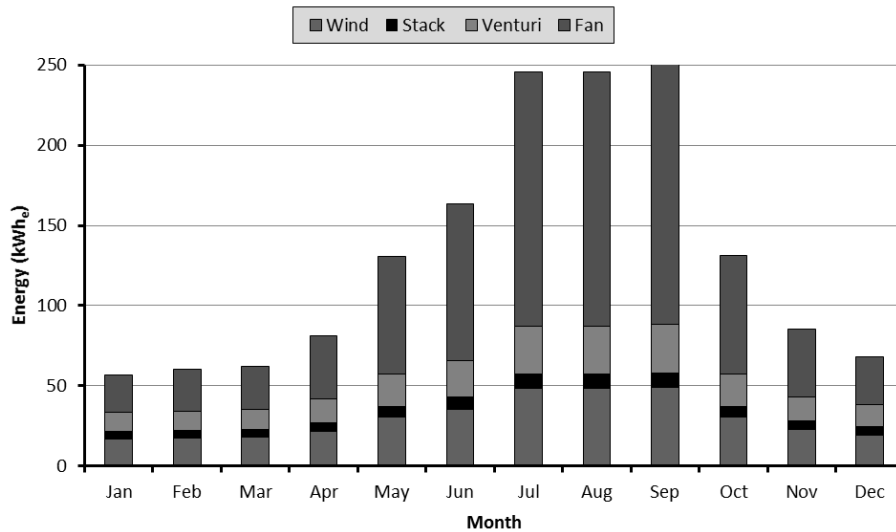


Figure 12. Single monthly trip energy contribution for each cooling approach in one chimney.

For the hybrid cooling system that is assumed blocked by the superstructure, produces a fuel reduction of around 32 kg in a single monthly trip. After the fan ventilation, the largest contributor to the condenser cooling comes from the stack flow rate which represents between 4.9% and 12.1%, depending on the month. Volumetric flow rates from the windscoops and Venturi-shaped roof are assumed to only be active when there are headwinds or tailwinds reducing considerably their benefits. Wind and roof cooling represent 1.6% and 1.1% of the total energy required respectively in January.

5. Discussion

This analysis did not include an evaluation of a potential increase in wind resistance due to the chimneys, as wind resistance is typically 4.0% or less of the ships total resistance [43], and the indicative system described only increases the projected area by 4.5% of the ship superstructure.

In regards to the possible corrosion for the aluminium condenser unit, Sielski [74] discusses that bare hulls made of aluminium alloys of the series 5xxx has been operating for 30 years without visible corrosion. In the proposed hybrid system, the condenser unit will be located inside the ship's superstructure where it will be just exposed to moist air. Under this scenario the corrosion could be managed by galvanically isolating the aluminium from other steel structures as done between aluminium superstructures and steel hulls. This can be achieved by placing a high ohmic resistance material (e.g. neoprene) between the heat exchanger and the steel deck as well as insulating sleeves and washers were needed. Other options mentioned by Vargel [75] are painting the surface in contact with other metals and by using sacrificial anodes (e.g. Zinc).

The windscoops have shown to be one of the largest contributors for the passive cooling system, but were subject to several assumptions. Examining the assumed opening effectiveness, Buklin et al. [76] gives opening effectiveness values as guidance for wind angles to the opening's surface between 10° and 90° based on [68]. In the arctic ORC study the opening effectiveness was assumed to be constant, and only the longitudinal component of the apparent velocity ($v_{a,l}$) was assumed to be captured by the windscoops. Re-examining these two assumptions it was found that the windscoops had, on average, a 4.3% larger opening effectiveness through the complete angle range. It is important to note that the values for the opening effectiveness in Buklin et al. [76] are given for any opening shape and structure. Also, the set of values in Buklin et al. for the opening effectiveness are given as constant for different wind angle range while in this work the combination of the opening effectiveness and the longitudinal component of the apparent velocity gives a continuous behaviour. Nääs et al. [77] showed that the opening effectiveness for a rectangular opening changes depending on the shape and structure of the opening. But it was also demonstrated that the opening effectiveness is more sensitive to a change in wind speed, dropping when faster winds arrive at the opening. In this work the effect of the speed on the windscoops was not considered. This will have an important impact on the system performance when there are fast headwinds (above 8 m/s), but as seen in Table 3 these types of winds have a low probability of occurring. The shape and structure of the opening tested by Nääs et al. is different than in this work, and as highlighted by Nääs et al. it is important to study the impact of the windscoop design on its performance for different wind angles and speeds.

For the Venturi-shaped roofs it was assumed a constant pressure coefficient of -0.75 for the whole AWA. Van Hooff et al. [34] found experimentally that a building omnidirectional Venturi-shaped roof without guiding vanes had a pressure coefficient (C_p) that fluctuated between -1.33 and -1.05 for TWA between 0° and 45°. From Equation (15) it is possible to see that larger C_p will increase the flow rate for the Venturi-shaped roofs. However, due to possible blockages in the ship superstructure, the flow may be disturbed and C_p may drop, hence the conservative value used in this study was deemed adequate. Similar to the windscoops, there is an important area of research on the Venturi-shaped roofs in regards to their shape. In this study, the roof designed by Van Hooff et al. [34] was adopted but reduced in its dimensions to fit them on the ship superstructure. However, Grant et al. [70] experimented with an omnidirectional spherical-shaped Venturi-roof achieving C_p between -2.5 and -2.2, almost three times higher than ones used in this work. Studying the performance of different shapes for Venturi-roofs along with the wind behaviour on the ship superstructure may reduce the need of the condenser's fan.

It was assumed that when wind arrived to one side of the superstructure, the windscoops on the other side will suffer from blockage due to the superstructure in their current location. Other locations for the windscoops, such as the superstructure roof, may entail much greater ducting losses but this could be offset by reduced sensitivity to apparent wind direction. Similarly, the local airflow near windscoops and Venturi devices may be degraded by the presence of fittings and masts or in the case of container ships, cargo. Ships such as tankers, carrying no deck cargo, may be able to employ windscoops over

a wider range of AWA, however. The initial analysis presented here has also assumed straight and smooth ducts, with a minimum of losses. Climate data has been averaged over a month and the study does not model the day-to-day variations of the day night variations in wind or temperature. On an even shorter time scale ship motion could impact results, for example, ship roll could impact apparent wind velocity and opening effectiveness.

In regards to the system integration to the ship, internal duct temperatures will be sufficiently low to permit light construction similar to HVAC ducting, with the mass of such a duct being approximately 75 kg/m in steel. This gives an added mass of 2.9 t for two ducts alone – not including the Venturi structure. If the ducts were constructed of aluminium, this could be reduced to one tonne for two ducts, or potentially less with foil-based flexible ducts. The lighter options would not be self-supporting however, being suspended from the superstructure bulkheads. Arranging the ducts inside the superstructure would be relatively straightforward, as most cargo vessels have a single centreline engine casing / funnel aft of the full width superstructure, so the ducts would be located outboard of this. Consideration of navigation radar arcs would be required for the choice of the Venturi-shaped roof height.

An interesting point of discussion is regarding fan isentropic efficiency which was assumed at a constant 60%. If the efficiency were to be increased to 80% the fuel savings for the same design will go to 1.9 t of fuel or 6.0 t less of CO₂. More interestingly, will be to observe if there are other more optimum ORC design – which return larger emission reductions – when the optimisation process is ran again with a higher fan isentropic efficiency. This possible scenario could bring the case forward for more research to be done in improving fan efficiency. On regards to the pump isentropic efficiency at design point, if it was to be reduced to 50%, the net electrical power output drops around 1% for all speeds. This will reduce the annual CO₂ emission from the ORC unit to 538 t per year rather than 543 t which represents the emissions reduced by using the hybrid cooling system. With a 65% pump isentropic efficiency, the net electrical power output drops to 0.4% with a reduction on annual CO₂ emissions from the ORC unit of 2.3 t which represents 47% of the CO₂ reduced by the hybrid cooling system.

Conclusions

The potential fuel and emissions savings for a containership navigating in the low Arctic from the installation of a forced-air-cooled ORC unit assisted by a passive cooling system was investigated. It was found that the ORC unit being cooled by air forced by a fan could reduce the vessel CO₂ annual emissions by 543 t/year. A twin passive cooling system with windscoops, Venturi-shaped roofs and chimneys improved the CO₂ emission reductions by 0.9%, or 1.6 t fuel/year. Comparing to the base case, the annual CO₂ emission reductions achieved by the hybrid cooling system reached 548 t which represents 0.92% of the containership annual CO₂ emissions or 9.80% of the auxiliary machinery annual CO₂ emissions.

The lowest fan electric power consumption, 2.2 kW_e, is achieved in January when the ship is navigating at 21 knots. At a speed of 24.6 knots and in September, the fan electric power input increases to its maximum of 48.6 kW_e. Wind cooling was the largest source of fan power reductions followed by Venturi-induced cooling and stack-induced cooling. The amount of induced flow rate by the hybrid system has been shown to depend on engine loading, apparent wind angle and speed. Under headwinds above 10 m/s at 23.3 knots and in the winter months, the cooling demand is wholly covered by the hybrid system while navigating at the highest speed at summer and the wind flow blocked by the ship superstructure represents 3.4% of the required electric power to cool down the ORC unit condenser. The required volume flow rate is sensitive to ambient air temperature. During the colder months and for an unblocked system, the passive cooling system had a larger contribution to the fan power reduction mainly caused by lower power demand at the condensers. For the summer months, the fan power requirement increases considerably while the volumetric flow rate of the roof and stack cooling reduces. However, it was found that the energy contributions are higher during the warmer months due to the fan power requirement from 0.09 kW_e/(m³/s) in January to 0.22 kW_e/(m³/s) in September. For the blocked hybrid system, the largest hybrid cooling contribution comes from the stack volumetric flow rate representing a maximum of 12.1%.

Further work is required to evaluate pressure losses in ducting and leakages into the optimisation process, equipment performance analysis and to improve the hybrid equipment ship integration, in particular the possibility of improving passive cooling performance by exploration of options and optimisation of design and location.

Acknowledgement

Special thanks to Ben Howett from University of Strathclyde for the processing and sharing of wind data for the Arctic route. Also, thanks to Dr Julia Schaumeier for her work on processing the navigational data for the case study vessel in the Arctic in her time at UCL's Energy Institute.

References

- [1] Aksenov Y, Popova EE, Yool A, Nurser AJG, Williams TD, Bertino L, et al. On the future navigability of Arctic sea routes: High-resolution projections of the Arctic Ocean and sea ice. *Mar Policy* 2017;75:300–17. doi:10.1016/j.marpol.2015.12.027.
- [2] National Snow And Ice Data Center. Sea Ice Index 2013:1. http://nsidc.org/data/seaice_index/ (accessed December 12, 2013).
- [3] Rogers TS, Walsh JE, Rupp TS, Brigham LW, Sfraga M. Future Arctic marine access: analysis and evaluation of observations, models, and projections of sea ice. *Cryosph* 2013;7:321–32. doi:10.5194/tc-7-321-2013.
- [4] Stephenson SR, Smith LC, Agnew JA. Divergent long-term trajectories of human access to the Arctic. *Nat Clim Chang* 2011;1:156–60. doi:10.1038/nclimate1120.
- [5] Schøyen H, Bråthen S. The Northern Sea Route versus the Suez Canal: cases from bulk shipping. *J Transp Geogr* 2011;19:977–83. doi:10.1016/j.jtrangeo.2011.03.003.
- [6] Melia N, Haines K, Hawkins E. Sea ice decline and 21st century trans-Arctic shipping routes. *Geophys Res Lett* 2016;43:9720–8. doi:10.1002/2016GL069315.
- [7] McGrath M. First tanker crosses northern sea route without ice breaker. *Br Broadcast Corp* 2017:1. <http://www.bbc.com/news/science-environment-41037071> (accessed December 18, 2017).
- [8] International Maritime Organization. MEPC 63/INF .2. 2011.
- [9] Eide MS, Endresen Ø, Skjong R, Longva T, Alvik S. Cost-effectiveness assessment of CO2 reducing measures in shipping. *Marit Policy Manag* 2009;36:367–84. doi:10.1080/03088830903057031.
- [10] Larsen U, Haglind F, Oskar S. A comparison of advanced heat recovery power cycles in a combined cycle for large ships. 26th Int. Conf. Effic. Cost, Optim. Simul. Environ. Impact Energy Syst., Guilin: Chinese Society of Engineering Thermophysics; 2013, p. 13.
- [11] Benvenuto G, Campora U, Trucco A. Comparison of ship plants layouts for power propulsion systems with energy recovery. 12th Int. Nav. Eng. Conf. Exhib., Amsterdam: Institute of Marine Engineering, Science and Technology; 2014, p. 329–40.
- [12] Suárez de la Fuente S. Reducing Shipping Carbon Emissions under Real Operative Conditions: A Study of Alternative Marine Waste Heat Recovery Systems based on the Organic Rankine Cycle. UCL, 2016.
- [13] Lloyd's Register. Provisional Rules for the Winterisation of Ships 2012 2012:104.
- [14] Woodyard D. Pounder's Marine Diesel Engines and Gas Turbines. 9th ed. Oxford: Butterworth-Heinemann; 2009.
- [15] Mito MT, Teamah MA, El-Maghlany WM, Shehata AI. Utilizing the scavenge air cooling in improving the performance of marine diesel engine waste heat recovery systems. *Energy* 2018;142:264–76. doi:10.1016/J.ENERGY.2017.10.039.

- [16] Shu G, Liang Y, Wei H, Tian H, Zhao J, Liu L. A review of waste heat recovery on two-stroke IC engine aboard ships. *Renew Sustain Energy Rev* 2013;19:385–401. doi:10.1016/j.rser.2012.11.034.
- [17] MAN Diesel & Turbo. Engine room and performance data for 12G95ME-C9.5-TII with part load engine control tuning (ECT) tuning 2014:9.
- [18] Vanslambrouck B, Vankeirsbilck I, Gusev S, Paepe M De. Efficiency comparison between the steam cycle and the organic Rankine cycle for small scale power generation. *Renew. Energy World Conf. Expo North Am.*, vol. 32, Long Beach: Howeast, Universiteit Gent,; 2012, p. 13.
- [19] Yang M-H, Yeh R-H. Thermo-economic optimization of an organic Rankine cycle system for large marine diesel engine waste heat recovery. *Energy* 2015;82:256–68. doi:10.1016/j.energy.2015.01.036.
- [20] Quoilin S, Broek M Van Den, Declaye S, Dewallef P, Lemort V. Techno-economic survey of Organic Rankine Cycle (ORC) systems. *Renew Sustain Energy Rev* 2013;22:168–86. doi:10.1016/j.rser.2013.01.028.
- [21] Suárez de la Fuente S, Larsen U, Pierobon L, Kærn MR, Haglind F, Greig A. Selection of cooling fluid for an organic Rankine cycle unit recovering heat on a container ship sailing in the Arctic region. *Energy* 2017;141:975–90. doi:10.1016/j.energy.2017.09.125.
- [22] Kalikatzarakis M, Frangopoulos CA. Multi-criteria selection and thermo-economic optimization of Organic Rankine Cycle system for a marine application. *Int J Thermodyn* 2015;18:133–41. doi:10.5541/ijot.75305.
- [23] Shu G, Liu P, Tian H, Wang X, Jing D. Operational profile based thermal-economic analysis on an Organic Rankine cycle using for harvesting marine engine's exhaust waste heat. *Energy Convers Manag* 2017;146:107–23. doi:10.1016/j.enconman.2017.04.099.
- [24] United Nations Environment Programme. Decisions Adopted by the Nineteenth Meeting of the Parties to the Montreal Protocol on Substances that Deplete the Ozone Layer 2007.
- [25] United Nations Environment Programme. Issues for discussion by and information for the attention of the Open-ended Working Group of the Parties to the Montreal Protocol at its resumed thirty-eighth meeting 2016:18.
- [26] Khan N, Su Y, Riffat SB. A review on wind driven ventilation techniques. *Energy Build* 2008;40:1586–604. doi:10.1016/J.ENBUILD.2008.02.015.
- [27] Tong Z, Chen Y, Malkawi A. Estimating natural ventilation potential for high-rise buildings considering boundary layer meteorology. *Appl Energy* 2017;193:276–86. doi:10.1016/J.APENERGY.2017.02.041.
- [28] Gil-Baez M, Barrios-Padura Á, Molina-Huelva M, Chacartegui R. Natural ventilation systems in 21st-century for near zero energy school buildings. *Energy* 2017;137:1186–200. doi:10.1016/J.ENERGY.2017.05.188.
- [29] Hiyama K, Glicksman L. Preliminary design method for naturally ventilated buildings using target air change rate and natural ventilation potential maps in the United States. *Energy*

- 2015;89:655–66. doi:10.1016/J.ENERGY.2015.06.026.
- [30] Medved S, Babnik M, Vidrih B, Arkar C. Parametric study on the advantages of weather-predicted control algorithm of free cooling ventilation system. *Energy* 2014;73:80–7. doi:10.1016/J.ENERGY.2014.05.080.
- [31] Wang W, Zhang H, Liu P, Li Z, Lv J, Ni W. The cooling performance of a natural draft dry cooling tower under crosswind and an enclosure approach to cooling efficiency enhancement. *Appl Energy* 2017;186:336–46. doi:10.1016/J.APENERGY.2016.02.007.
- [32] Saadatian O, Haw LC, Sopian K, Sulaiman MY. Review of windcatcher technologies. *Renew Sustain Energy Rev* 2012;16:1477–95. doi:10.1016/j.rser.2011.11.037.
- [33] Hughes BR, Calautit JK, Ghani SA. The development of commercial wind towers for natural ventilation: A review. *Appl Energy* 2012;92:606–27. doi:10.1016/j.apenergy.2011.11.066.
- [34] van Hooff T, Blocken B, Aanen L, Bronsema B. A venturi-shaped roof for wind-induced natural ventilation of buildings: Wind tunnel and CFD evaluation of different design configurations. *Build Environ* 2011;46:1797–807. doi:10.1016/j.buildenv.2011.02.009.
- [35] Containership-Info. JPO LIBRA 2014:1. <http://www.containership-info.com/> (accessed September 22, 2014).
- [36] Clarkson Research Services Limited. Shipping Intelligence Network 2013.
- [37] MAN Diesel & Turbo. Engine room and performance data for 8S90ME-C9.5-TII with high load tuning. 2015:10.
- [38] Smith TWP, Jalkanen JP, Anderson BA, Corbett JJ, Faber J, Hanayama S., et al. Third IMO GHG Study 2014. London: 2014.
- [39] Jones PD, Lister DH, Osborn TJ, Harpham C, Salmon M, Morice CP. Hemispheric and large-scale land-surface air temperature variations: An extensive revision and an update to 2010. *J Geophys Res* 2012;117:D05127. doi:10.1029/2011JD017139.
- [40] Jones PD, New M, Parker DE, Martin S, Rigor IG. Surface air temperature and its changes over the past 150 years. *Rev Geophys* 1999;37:173. doi:10.1029/1999RG900002.
- [41] Dee DP, Uppala SM, Simmons AJ, Berrisford P, Poli P, Kobayashi S, et al. The ERA-Interim reanalysis: configuration and performance of the data assimilation system. *Q J R Meteorol Soc* 2011;137:553–97. doi:10.1002/qj.828.
- [42] Ship Structure Committee. SSC-406: Sea Operational Profiles For Structural Reliability Assessment. Washington DC: 1999.
- [43] Molland AF, Turnock SR, Hudson DA. Ship Resistance and Propulsion. 1st ed. New -York: Cambridge University Press; 2011.
- [44] Datla BV, Brasz J. Comparing R1233zd and R245fa for Low Temperature ORC Applications. *Int. Refrig. Air Cond. Conf.*, Purdue: Purdue University; 2014, p. 7.
- [45] Honeywell. Solstice © 1233zd (E) Safety Data Sheet 2014:1–14.
- [46] International Maritime Organization. SOLAS, Consolidated Edition 2009. 5th ed. London: IMO Publishing; 2009.

- [47] Hulse RJ, Basu RS, Singh RR, Thomas RHP. Physical Properties of HCFO-1233zd(E). *J Chem Eng Data* 2012;57:3581–6. doi:10.1021/je300776s.
- [48] Shah RK, Sekulic DP. *Fundamentals Of Heat Exchanger Design*. 1st ed. New Jersey: John Wiley & Sons, Inc.; 2003.
- [49] Yun L, Bliault A. *Manoeuvrability. Theory Des. Air Cushion Cr.* 1st ed., Oxford: Elsevier Butterworth-Heinemann; 2000, p. 205–31.
- [50] Calise F, Capuozzo C, Carotenuto A, Vanoli L. Thermo-economic analysis and off-design performance of an organic Rankine cycle powered by medium-temperature heat sources. *Sol Energy* 2014;103:595–609. doi:10.1016/j.solener.2013.09.031.
- [51] Sellers C. Field operation of a 125kW ORC with ship engine jacket water. *Energy Procedia*, vol. 129, Milan: Elsevier; 2017, p. 495–502. doi:10.1016/J.EGYPRO.2017.09.168.
- [52] Øien HA. *Energy efficient operation of ships*. Norwegian University of Science and Technology, 2011.
- [53] Xiros N. *Marine Engine Thermodynamics. Robust Control Diesel Sh. Propuls.* 1st ed., London: Springer-Verlag London Ltd.; 2002, p. 13–42. doi:10.1007/978-1-4471-0191-8_2.
- [54] Pierobon L, Benato A, Scolari E, Haglind F, Stoppato A. Waste heat recovery technologies for offshore platforms. *Appl Energy* 2014;136:228–41. doi:10.1016/j.apenergy.2014.08.109.
- [55] Walraven D, Laenen B, D'haeseleer W. Minimizing the levelized cost of electricity production from low-temperature geothermal heat sources with ORCs: Water or air cooled? *Appl Energy* 2015;142:144–53. doi:10.1016/j.apenergy.2014.12.078.
- [56] Nielsen RF, Haglind F, Larsen U. Design and modeling of an advanced marine machinery system including waste heat recovery and removal of sulphur oxides. *Energy Convers Manag* 2014:687–693. doi:10.1016/j.enconman.2014.03.038.
- [57] Chen Y, Lundqvist P, Johansson A, Platell P. A comparative study of the carbon dioxide transcritical power cycle compared with an organic rankine cycle with R123 as working fluid in waste heat recovery. *Appl Therm Eng* 2006;26:2142–7. doi:10.1016/j.applthermaleng.2006.04.009.
- [58] Larsen U, Pierobon L, Baldi F, Haglind F, Ivarsson A. Development of a model for the prediction of the fuel consumption and nitrogen oxides emission trade-off for large ships. *Energy* 2015;80:545–55. doi:10.1016/j.energy.2014.12.009.
- [59] Bao J, Zhao L. A review of working fluid and expander selections for organic Rankine cycle. *Renew Sustain Energy Rev* 2013;24:325–42. doi:10.1016/j.rser.2013.03.040.
- [60] Schobeiri M. *Turbine Aerodynamic Design and Off-design Performance*. Turbomach. Flow Phys. Dyn. Perform. 1st ed., Berlin, Heidelberg: Springer Berlin Heidelberg; 2005, p. 409–37. doi:10.1007/978-3-540-26591-7_17.
- [61] Cooke DH. On Prediction of Off-Design Multistage Turbine Pressures by Stodola's Ellipse. *J Eng Gas Turbines Power* 1985;107:596. doi:10.1115/1.3239778.
- [62] Suárez de la Fuente S, Roberge D, Greig AR. Safety and CO₂ emissions: Implications of

- using organic fluids in a ship's waste heat recovery system. *Mar Policy* 2017;75:191–203. doi:10.1016/j.marpol.2016.02.008.
- [63] International Maritime Organization. Resolution MEPC.212(63) - 2012 Guidelines On The Method Of Calculation Of The Attained Energy Efficiency Design Index (EEDI) For New Ships. 2012.
- [64] Larsen U, Pierobon L, Haglind F, Gabriellii C. Design and optimisation of organic Rankine cycles for waste heat recovery in marine applications using the principles of natural selection. *Energy* 2013;55:803–12. doi:10.1016/j.energy.2013.03.021.
- [65] Pierobon L, Larsen U, Haglind F, Elmegaard B, Nguyen T-V. Multi-objective optimization of organic Rankine cycles for waste heat recovery: Application in an offshore platform. *Energy* 2013;58:538–49. doi:10.1016/j.energy.2013.05.039.
- [66] Suárez de la Fuente S, Greig A. Making shipping greener: comparative study between organic fluids and water for Rankine cycle waste heat recovery. *J Mar Eng Technol* 2015;14:70–84. doi:10.1080/20464177.2015.1077601.
- [67] Bell IH, Wronski J, Quoilin S, Lemort V. Pure and Pseudo-pure Fluid Thermophysical Property Evaluation and the Open-Source Thermophysical Property Library CoolProp. *Ind Eng Chem Res* 2014;53:2498–508. doi:10.1021/ie4033999.
- [68] American Society of Heating Refrigerating and Air-Conditioning Engineers. 2013 ASHRAE handbook: Fundamentals. Atlanta: American Society of Heating Refrigerating and Air-Conditioning Engineers; 2013.
- [69] Albright LD. Environment control for animals and plants / Louis D. Albright. - Version details - Trove. 1st ed. St Joseph: ASAE Publishing; 1990.
- [70] Grant EJ, Jones JR, Vlachos PP. Design and Wind Tunnel Performance Testing of a New Omnidirectional Roof Vent. *J Archit Eng* 2007;13:18–21. doi:10.1061/(ASCE)1076-0431(2007)13:1(18).
- [71] Walker IS, Wilson DJ. Evaluating models for superposition of wind and stack effect in air infiltration. *Build Environ* 1993;28:201–10. doi:10.1016/0360-1323(93)90053-6.
- [72] Richardson JF, Peacock DG. Coulson and Richardson's Chemical Engineering Volume 3 - Chemical and Biochemical Reactors and Process Control. 3rd ed. Oxford: Elsevier; 1994.
- [73] Gnielinski V. G7 Heat Transfer in Cross-flow Around Single Rows of Tubes and Through Tube Bundles. In: VDI-Gesellschaft Verfahrenstechnik und Chemieingenieurwesen, editor. VDI Heat Atlas. 2nd ed., Düsseldorf: Springer-Verlag Berlin Heidelberg; 2010, p. 725–30.
- [74] Sielski RA. Research needs in aluminum structure*. *Ships Offshore Struct* 2008;3:57–65. doi:10.1080/17445300701797111.
- [75] Vargel C. Corrosion of aluminium. 1st ed. Oxford: Elsevier; 2004.
- [76] Bucklin RA, Nääs IA, Zazueta FS, Walker WR. Natural ventilation in swine housing - *Bulletin* 270 1991:38.
- [77] Nääs IA, Moura DJ, Bucklin RA, Fialho FB. An algorithm for determining opening effectiveness

in natural ventilation by wind. Trans ASAE 1998;41:767–71.